COMMUNICATIONS CHEMISTRY

ARTICLE

https://doi.org/10.1038/s42004-019-0241-1 OPEN

Flow chemistry controls self-assembly and cargo in Belousov-Zhabotinsky driven polymerization-induced self-assembly

Liman Hou[1], Marta Dueñas-Díez[1,2*], Rohit Srivastava[1] & Juan Pérez-Mercader[1,3*]

Amphiphilic block-copolymer vesicles are increasingly used for medical and chemical applications, and a novel method for their transient self-assembly orchestrated by periodically generated radicals during the oscillatory Belousov-Zhabotinsky (BZ) reaction was recently developed. Here we report how combining this one pot polymerization-induced self-assembly (PISA) method with a continuously stirred tank reactor (CSTR) strategy allows for continuous and reproducible control of both the PISA process and the chemical features (e.g. the radical generation and oscillation) of the entrapped cargo. By appropriately tuning the residence time (τ), target degree of polymerization (DP) and the BZ reactants, intermediate self-assembly structures are also obtained (micelles, worms and nano-sized vesicles). Simultaneously, the chemical properties of the cargo at encapsulation are known and tunable, a key advantage over batch operation. Finally, we also show that BZ-driven polymerization in CSTR additionally supports more non-periodic dynamics such as bursting.

[1] Department of Earth and Planetary Sciences and Origins of Life Initiative, Harvard University, Cambridge, MA 02138-1204, USA. [2] Repsol Technology Lab, c/ Agustín de Betancourt, s/n, 28935 Móstoles, Madrid, Spain. [3] Santa Fe Institute, Santa Fe, NM 87501, USA. *email: marta.duenas@repsol.com; jperezmercader@fas.harvard.edu

Amphiphilic block copolymer vesicles (or polymersomes)[1,2] have emerged as attractive artificial systems mimicking basic properties thought to be present in primitive cell membranes in the origin of life[3,4] and play a role in artificial life contexts[5,6]. Polymersomes are also becoming widely used as nanoreactors or nanocarriers[7,8]. Polymer vesicles are more stable, have stronger mechanical resistance, and their membranes are easier to functionalize than those of liposomes[9–13]. Polymerization-induced self-assembly (PISA) is a powerful one-pot one-solvent strategy to prepare well-defined polymer vesicles, and because of its autonomous character, it provides many novel opportunities in a variety of fields from active materials to artificial biology[14–19].

In a typical PISA setting, in a batch reactor, a soluble polymer is chain-extended with a second monomer to form amphiphilic diblock copolymers that can further undergo self-assembly into a range of morphologies[14,15]. Many polymerization methods have been used to perform PISA, including reversible addition–fragmentation chain transfer (RAFT)–PISA, atom transfer radical polymerization (ATRP)–PISA, ring-opening metathesis polymerization (ROMP)–PISA, enzymatic PISA, and others[20]. Recently, our group reported a novel RAFT–PISA approach, the Belousov–Zhabotinsky (BZ) reaction-driven RAFT–PISA, which shows significant activity for the synthesis of giant polymer vesicles under fully open-air conditions with water as a solvent[21,22].

The BZ reaction is the first and most studied nonbiochemical oscillatory reaction. It was first discovered in the 1950s by Belousov while he was looking for a chemistry-mimicking glycolysis[23,24]. The reaction involves the oxidation of a weak organic acid (e.g., citric acid and malonic acid) in an acidic aqueous solution in the presence of bromate ions and a transition metal catalyst that can oscillate between two oxidation states (e.g., Ce^{3+}–Ce^{4+} and Ru^{2+}–Ru^{3+}). The redox potential relaxation oscillations occur because the key intermediate bromide ions Br^- and the autocatalytically generated bromous acid $HBrO_2$ compete for the bromate ions. Figure 1c shows a simplified reaction mechanism of the BZ reaction (adapted from the Field–Körös–Noyes (FKN) mechanism[25]) and its interactions with the RAFT main equilibrium reaction.

The BZ reaction was later[26] experimentally shown to be caused by a free-radical mechanism by observing the inhibition of oscillations when in the presence of acrylonitrile monomers. In the course of an oscillation, as the catalyst is oxidized, bromine dioxide radicals are dominantly produced, while as the catalyst is reduced, malonyl radicals are dominantly produced[27]. Acrylonitrile polymerization by BZ chemistry was further studied both experimentally and mechanistically in a batch reactor[28]. PISA has been shown to take place when coupling the periodically generated radicals from an oscillating BZ reaction to chain- extend a hydrophilic PEG macroCTA to form an amphiphilic copolymer that further self-assembled into blebbing and dividing polymer vesicles[21,22]. Due to the autonomous nature of the self-assembly, the resulting polymer vesicles entrap the active oscillatory reaction and thus maintain not only the "living" property typical of RAFT, but also augments the functionality of the resulting vesicles with information-handling capabilities[22,29,30]. It should also be noted that the BZ chemical initiation of the polymerization has some advantages over thermal initiation, most of which are shared with photoinitiation methods: BZ is run at low temperatures (typically in the range 20–30 °C), is oxygen tolerant, runs in open-air conditions in aqueous medium, and the catalyst is not consumed during polymerization but continuously and periodically regenerated through the chemical oscillations. Indeed, the catalyst regeneration can be tuned to a large extent and through a variety of operating variables that influence radical production,

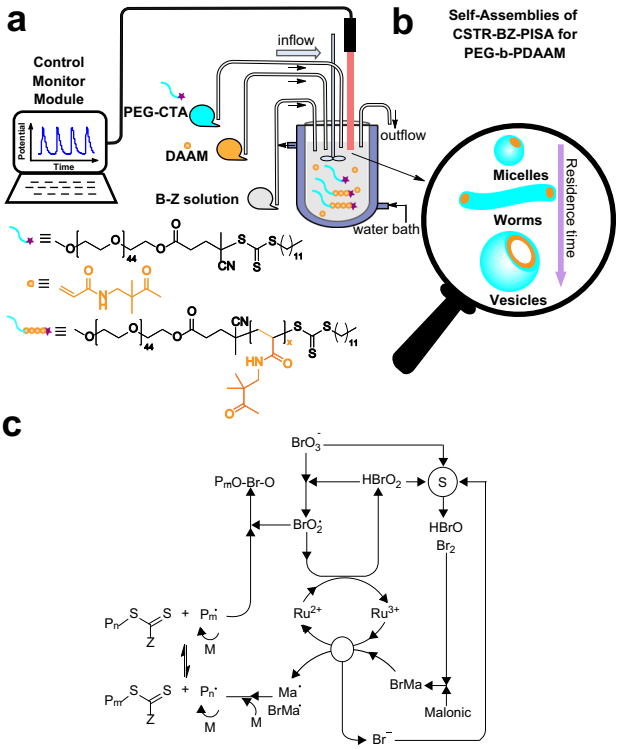

Fig. 1 Overview. Schematic representation of the CSTR setup, key reactants, self-assembled objects, and the kinetic mechanism. a Schematic illustration of the CSTR setup in which BZ reactants, monomer, and PEG macroCTA are continuously pumped into the reactor and products are continuously pumped out of the reactor to achieve constant volume and constant residence time. Redox potential is used to monitor in real time the transient and stationary oscillations. **b** The resulting self-assemblies of BZ reaction-mediated aqueous RAFT dispersion polymerization of DAAM to form PEG-b-PDAAM. **c** Simplified mechanism[25] of the BZ reaction coupled to the main RAFT equilibrium. Here, BrMa* is bromomalonic acid, Ma malonyl radicals, BrMa* bromomalonyl radicals, and S represents a subnetwork of reactions not shown for simplicity[25].

including temperature, BZ reactants, stirring rate, light intensity, and wavelength. Note that the cargo we want to encapsulate also drives the polymerization while not requiring additional initiators.

Our motivation in choosing CSTR operation for BZ–PISA is to simultaneously control in a consistent and repeatable way both the PISA process and the chemical features (i.e., the period, amplitude, and shape of oscillations) of the entrapped cargo. In a batch operation, the BZ reaction will eventually reach equilibrium and cause the oscillations to die out, therefore strongly affecting the dynamics of the radical species. A more critical challenge is that in batch it is literally impossible to know accurately the chemical properties of the entrapped cargo at self-assembly, since the features of the oscillations are continuously varying as the polymerization progresses. In contrast, a CSTR operation with the continuous inflow of reactants and outflow of the reaction media allows for keeping indefinitely the system in a stationary out-of-equilibrium oscillatory mode with well-defined and precisely known oscillatory features, and hence, the associated radical dynamics. BZ in CSTR operation mode has been widely studied since the 1970s[31–36]. Initial work focused on evaluating the conditions in which oscillations can be sustained and demonstrated that there is a range of residence times over which they occur[31], and also that near the lower end and higher end of this range, more complex oscillatory behaviors[32] exist such as

multipeaked periodic oscillations, bursting patterns, high sensitivity to small perturbations, or deterministic chaos[33–35]. It has recently been reported that feed rate noise can also modulate autocatalysis and shapes of the oscillations of the BZ reaction in CSTR[37]. Thus, coupling BZ–PISA with the CSTR operation of BZ holds great potential for achieving better control and consistency of both the self-assembled vesicles and their encapsulated cargo.

Interest in running PISA in continuous reactors is growing rapidly[38–45] with the focus placed on plug-flow reactors and their variants such as slug flow[45], since such mode of operation leads to the narrowest residence time distributions, and with it to the tightest control of the final polymer length distribution and self-assembled objects. However, a plug-flow reactor is not adequate for our purpose because when BZ is run in plug flow, it results in stationary space-periodic structures ("waves")[46] with constant forcing at the inflow and to traveling space-periodic waves with periodic forcing at the inflow[47], and our focus is on encapsulating temporal–periodic oscillations and not space-periodic oscillations.

Here we show the autonomous synthesis of polymer vesicles with an active encapsulated and tunable BZ oscillatory reaction, making use of a novel PISA CSTR mode of operation and achieving simultaneous control of the self-assembly and the cargo properties.

Results

Macro-chain transfer agent synthesis and functionalization. First, a water-soluble PEG_{45}-4-cyano-4-[(dodecylsulfanylthiocarbonyl) sulfanyl]pentanoic acid was synthesized and used as macro-chain transfer agent (macroCTA) and stabilizing block[48]. The functionalization of PEG–OH with small RAFT molecules to synthesize our macroCTA was determined to be 98% using ^{1}H NMR spectroscopy (Supplementary Fig 1).

Continuously stirred tank reactor operation. Commercially available diacetone acrylamide (DAAM) was used as a monomer known to be water-miscible at room temperature, yet its polymer is water-insoluble and has previously been reported to be a monomer for PISA[49,50]. As mentioned in the introduction, the oscillating BZ reaction can generate radicals periodically to initiate the polymerization of the monomer[26–28]. Figure 1a illustrates schematically the CSTR setup where the BZ reactants, monomer, and PEG-based macroRAFT are continuously pumped into the reactor, and the products are pumped out continuously to maintain a constant volume. In the reactor, as the PDAAM block grows to a critical length, the diblock copolymer self-assembles in water to form polymer objects (Fig. 1b). Samples for further analysis were collected both at specific time intervals and after the oscillations stabilized (after 1.5 times the residence time).

Oscillatory redox potential profiles for different reactor modes. Figure 2 illustrates the differences between the redox oscillatory features of batch versus CSTR operation of both the pure BZ reaction and its course when providing radicals for PISA. Note how the oscillatory features vary considerably with time in the case of batch operation (see Fig. 2a, c), while in CSTR, the chemical oscillation features reach stationary periodicity both in pure BZ and in BZ-driven polymerization (see Fig. 2b for pure BZ reaction and Fig. 2d for BZ–PISA). In batch, the presence of monomer and macroCTA leads to considerably longer induction times, considerably shorter time span in the oscillatory regime, and different transient trends in the oscillatory features, i.e., the average and period of each oscillation compared with the same observed trends for BZ alone. The induction time here increased to ~3000 s due to the PEG macroCTA and monomer (Fig. 2c). The presence of monomer and macroCTA in CSTR operation changed the oscillatory features but reached, as expected, stationary conditions that guarantee a controlled stationary supply of radicals for polymerization. The stationary oscillations in Fig. 2d have a stable period of ~42 s and a stable amplitude of ~100 mV compared with the pure BZ reaction without any of the RAFT ingredients (the period was about ~45 s and the amplitude ~150 mV). All these CSTR results confirm that stable oscillations are reached, thus avoiding radical depletion and ensuring stable polymerization and self-assembly conditions.

The inflow concentration of reactants in CSTR matched the initial conditions of the batch experiments (0.2 mM Ru-catalyst recipe).

Characterization of the PEG-b-PDAAM block copolymer. Figure 3 presents the results of the characterization of the resulting PEG-b-PDAAM block copolymers. ^{1}H NMR and gel permeation chromatography (GPC) were used to confirm the formation of PEG-b-PDAAM. DAAM conversion by ^{1}H NMR was determined to be ~55% by comparison of the PEG signals at 3.64–3.675 ppm labeled "a" to the PDAAM methyl signal labeled "f" (Fig. 3a). The molecular weight (M_n) and molar mass dispersity index measured by GPC were ~4.2×10^4 g mol^{-1} and ~3.0 (Fig. 3b), respectively. (The broad molecular distribution is typical for CSTR because the lifetime of a growing/dormant polymer chain of a living process is equal to the residence time in the reactor[51].) Note that as the actual time any molecule spends in a CSTR follows a normal distribution whose dispersion grows as the residence time grows, the distribution of polymer chains and self-assembled objects is also expected to be broader at longer residence times.

To understand the effect of the BZ–CSTR operating variables on the polymerization, we monitored both the transient and steady-state conversion. The steady-state conversion was determined by ^{1}H NMR and involved a time-consuming purification process. For the transient monomer conversion, UV–vis spectroscopy was used by detecting the decline of the absorption of DAAM at $\lambda_{max} = 226$ nm, which derives from the conjugation effect between C=C and C=O of α,β-unsaturated amides, and disappears after being polymerized. The concentration standard plot of the DAAM monomer is shown in Supplementary Fig. 2 in the Supporting Information. Conversion dynamic trends for three different residence times (40, 90, and 120 min), BZ 0.2 mM Ru-catalyst recipe, and monomer/RAFT ratio of concentration of 400 are shown in Fig. 3c. Conversions increased rapidly within the first hour and then stabilized for each residence time. As residence time increases, so does conversion as is clearly seen in Fig. 3c.

Transient self-assembly evolution during CSTR operation. Morphological evolution during the transient CSTR operation was studied by transmission electron microscopy (TEM) (Fig. 4a–c). Micelles with a diameter of ~80 nm were first observed after 1800 s. As the reaction time progresses, the residence time effect becomes apparent. A mixture of micelles, small amounts of worms, and nanovesicles were obtained in the sample taken after 60 min. Finally, giant vesicles with a diameter ~2 μm were formed after the reaction reaches the 120-min coordinate. The morphology corresponding to the sample taken after 180 min, was thoroughly characterized by TEM (Fig. 4d), dynamic light scattering (DLS) (Fig. 4e), and confocal laser-scanning microscopy (CLSM) (Fig. 4f). The DLS results confirmed that micrometer-sized vesicles have been formed, while CLSM showed that hollow vesicles formed with a diameter that could be as large as ~5 μm.

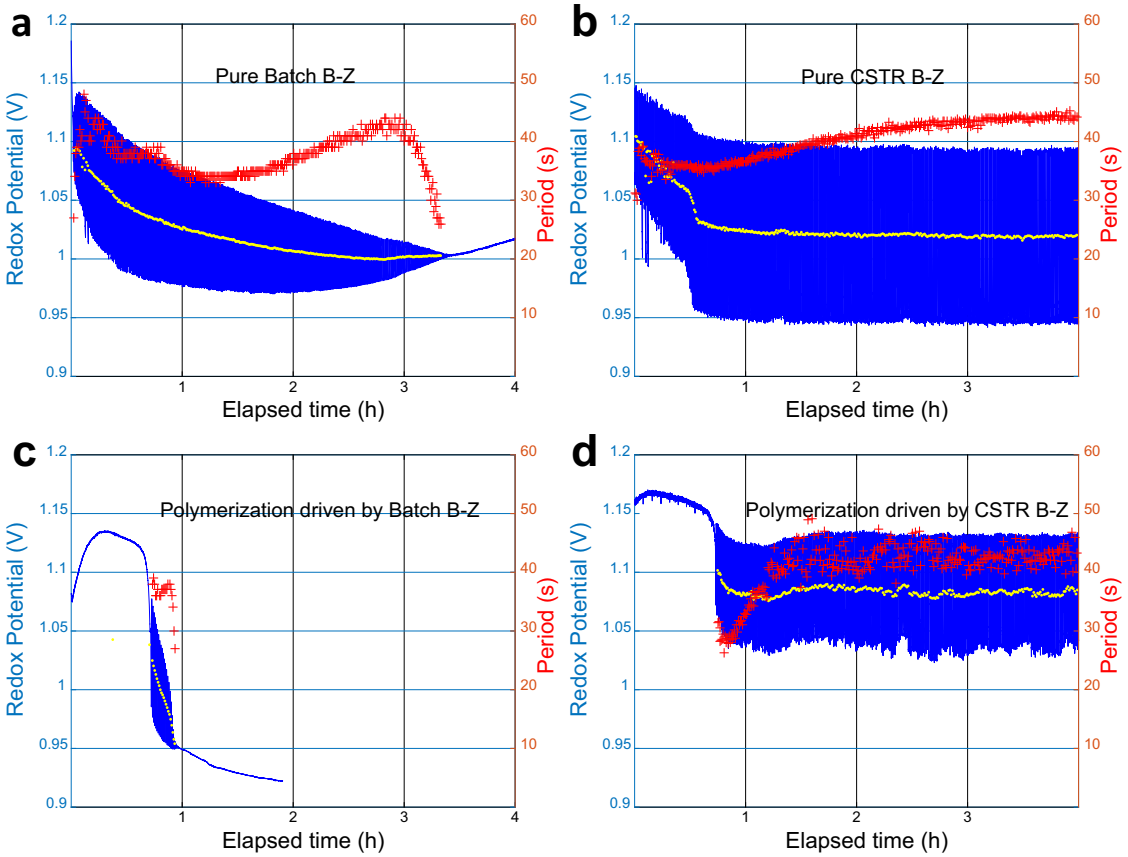

Fig. 2 Oscillatory redox potential profiles for different reactor configurations. Comparison of the redox potential measurements (in blue) and period of oscillations (in red) of pure BZ reaction in batch (panel **a**) and CSTR operation (panel **b**), in turn compared with polymerization driven by BZ reaction in batch (panel **c**) and CSTR (panel **d**).

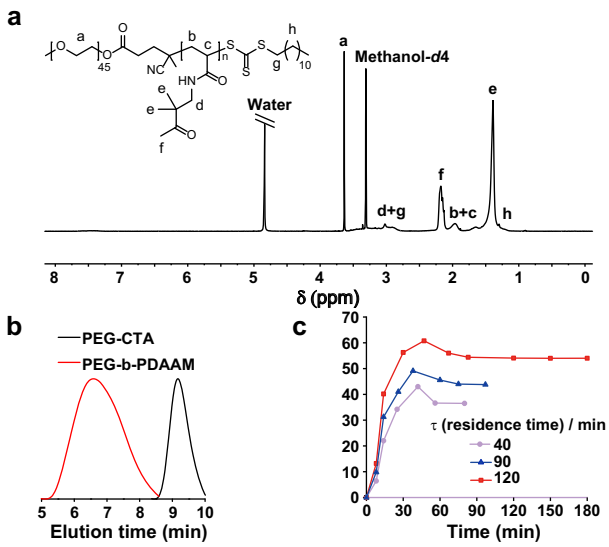

Fig. 3 Characterization of the resulting PEG-b-PDAAM block copolymer. ^{1}H NMR spectrum (**a**) and GPC (**b**) of the product at the steady state for the CSTR-BZ-PISA of PEG-b-PDAAM with a residence time (τ) of 120 min (sampled out at 180 min) and monomer/RAFT ratio of concentration = 400 at 1.1% w/w solid content. **c** Dynamic DAAM conversion versus time plot by UV–vis spectra for three experiments with the same theoretical target DP (400) and residence times of 40, 90, and 120 min, respectively.

Effect of residence time and of the monomer/RAFT ratio. In order to demonstrate the versatility of BZ–CSTR PISA, we targeted different morphologies by varying residence time after noticing that longer residence times imply larger conversions and larger lengths of the solvophobic block. Samples withdrawn 1.5 times the residence time were analyzed via TEM that revealed morphological transitions from spheres and worm mixtures (40-min residence time, Fig. 5a), to nanovesicles (90-min residence time, Fig. 5b), to finally GVs with diameters as large as ~2 μm (120-min residence time, Fig. 4d).

To further demonstrate the adaptability of the CSTR–BZ–PISA system, we investigated morphology changes by varying the monomer/RAFT ratio of concentrations. As shown in Fig. 5c, pure micelles were obtained at a residence time of 90 min, while worms (Fig. 5d) and spherical nanoaggregates (Fig. 5e) were obtained at longer residence times of 120 and 150 min. The final conversion values judged by UV–vis spectra were respectively 41.3%, 52.9%, and 55.6%, as summarized in Table 1. Compared with the results for a monomer/RAFT ratio of concentration of 400 (Fig. 5a, b), longer residence times are required to achieve equivalent self-assembled morphologies as the ratio was reduced.

Residence time as a consistent control variable. Of course, the residence time can be varied in a straightforward and rapid way by adjusting the pumped flowrates. Residence time is thus a convenient control variable if it can affect polymerization and self-assembly in an observable and reproducible manner. To prove such reproducibility experimentally, we ran an experiment in which the residence time was varied from 60 to 120 min and

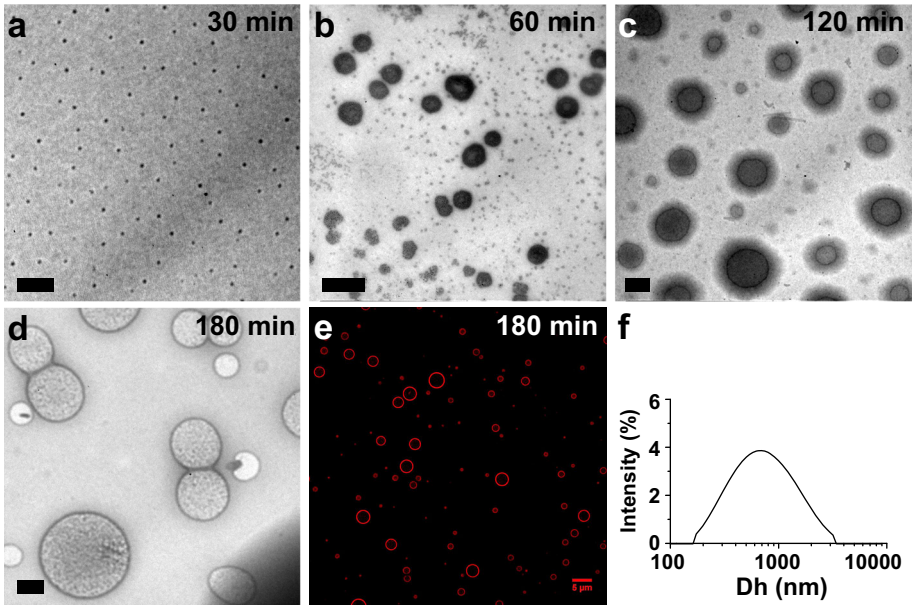

Fig. 4 Morphology characterization during transient CSTR conditions. Morphology characterization of the PEG-b-PDAAM self-assembled structures during transient CSTR conditions with a BZ 0.2 mM Ru-catalyst recipe, theoretical target DP of 400, and residence time of 120 min. Samples were taken at **a** 30 min (micelles), **b** 60 min (micelles, worms, and vesicles), and **c** 120 min (vesicles). Morphology characterization of the PEG-b-PDAAM vesicles sampled at 180 min by **d** TEM, **e** CLSM, and **f** DLS. All scale bars in the TEM images represent 500 nm.

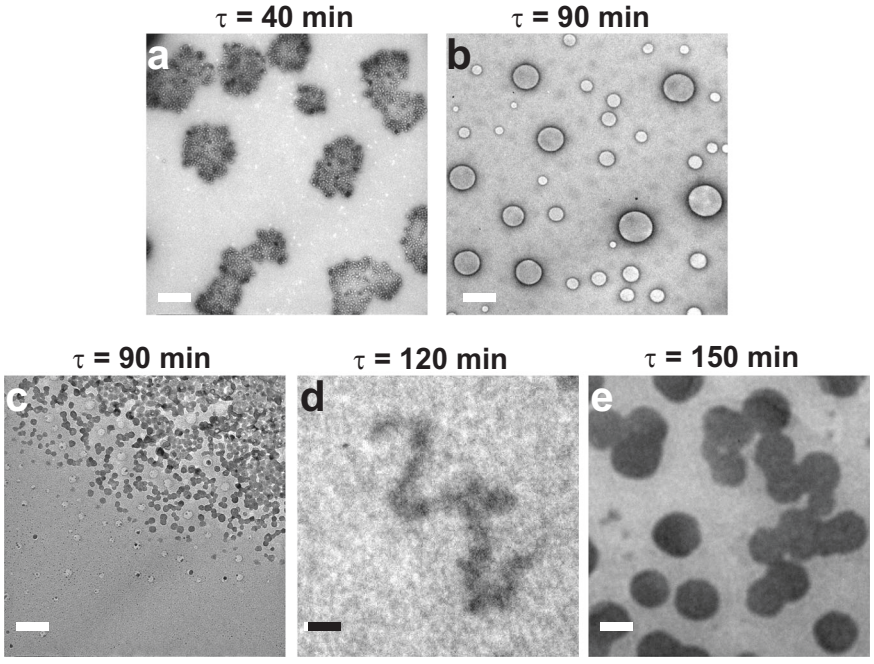

Fig. 5 Effect of residence time and monomer/RAFT ratio on self-assembly. Dominant morphology selection tuned by varying the residence time (panels **a, b** scale bar 500 nm) and monomer/RAFT ratio of concentrations (panels **c**–**e**, scale bar 100 nm), respectively. TEM images of PEG-b-PDAAM assemblies formed at residence times of 40 and 90 min (panels **a** and **b**). For comparison, samples were taken after 1.5 times the residence time at residence times of 90, 120, and 150 min when target DP was decreased to 200. In all cases, BZ 0.2 mM Ru-catalyst recipe was used.

back to 60 min. However, prior to running the experiment, we carried out some residence time distribution measurements to establish when steady state is attained in our setup. Due to the difficulty of finding an inert tracer for BZ, we ran the measurements with water as flowing medium and a fluorescent tracer. From this, we concluded that an elapsed time equivalent to three residence times is needed to reach steady state (see Supplementary Figs. 3 and 4). Supplementary Fig. 5 shows the oscillations of the redox potential of the B–Z reaction. The reaction oscillated with average period and amplitude of ~36 s and ~120 mV, respectively, at residence time of 60 min. Interestingly, when the residence time was changed to 120 min in stage 2, a bursting/chaotic behavior of the redox potential was observed instead of the expected periodic oscillations. Once the setpoint was reduced back to 60 min, the bursting behavior was substituted by an oscillatory behavior equivalent to that of the beginning of the

Table 1 Polymerization and self-assembly for CSTR-BZ-PISA of PEG-b-PDAAM with different residence times (τ), target DPs, and BZ recipes.

Exp.	DP	BZ recipe[a] (mM)	T (min)	Con.[b] (%)	Morphology[c]
1	400	0.2	40	36.5	M + W
2	400	0.2	60	40.9	nanoV
3	400	0.2	90	43.8	nanoV
4	400	0.2	120	53.7	GVs
5	200	0.2	60	37.3	-
6	200	0.2	90	41.3	M
7	200	0.2	120	52.9	W
8	200	0.2	150	55.6	SA
9	200	0.45	60	43.1	M + W
10	200	0.45	120	57.7	GVs

[a]Reagents and concentrations in the reactor: BZ 0.2 mM Ru-catalyst recipe (Ru $(bpy)_3^{2+}$, 0.2 mM; $NaBrO_3$, 150 mM; H_2SO_4, 500 mM; $CH_2(COOH)_2$, 60 mM) and BZ 0.45 mM Ru-catalyst recipe (Ru $(bpy)_3^{2+}$, 0.45 mM; $NaBrO_3$, 300 mM; H_2SO_4, 900 mM; $CH_2(COOH)_2$, 90 mM)
[b]Monomer conversions taken as steady-state values were determined via UV–vis spectroscopy
[c]Morphology was observed by TEM analysis: *M* micelles, *W* worms, *SA* sphere nanoaggregates, *nanoV* nanosized vesicles, *GVs* giant vesicles

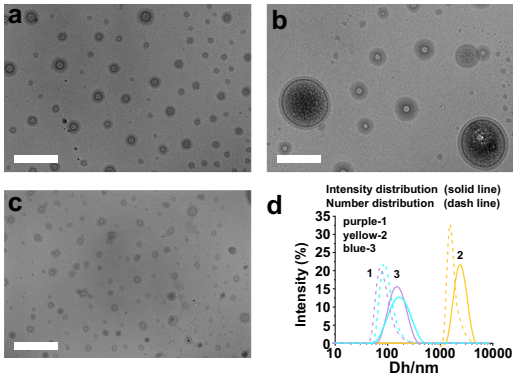

Fig. 6 Residence time as a control variable. Experiment designed to test for the consistency of oscillatory features and dominant self-assembly when residence time is used as control variable, first increased and then decreased to the original value (τ) (stages 1 and 3: $\tau = 60$ min, stage 2: $\tau = 120$ min). TEM images for samples from stages 1 (**a**), 2 (**b**), and 3 (**c**), respectively, all scale bars represent 1 μm. DLS results (intensity and number distributions) for the three stages (**d**).

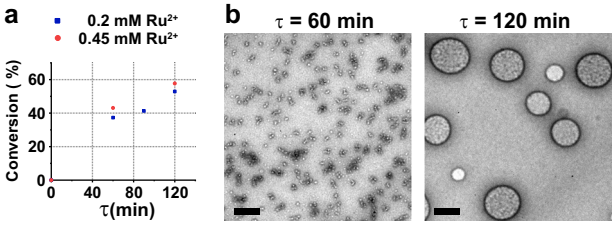

Fig. 7 Effect of BZ-reactant recipe on self-assembly. a Comparison of conversion calculated by UV–vis as a function of residence time for 0.45 mM Ru-catalyst recipe (orange sphere) compared with 0.2 mM Ru-catalyst recipe (navy blue square). **b** TEM images with 0.45 mM Ru-catalyst recipe (target DP = 200). The scale bars represent 500 nm.

experiment. Regarding the polymer morphology, nanovesicles were obtained at residence time of 60 min in the first stage and in the last stage having, as expected, similar average sizes of ~150 nm as can be seen from both TEM images (Fig. 6a, c) and DLS (Fig. 6d, and Supplementary Table 2). It is noteworthy that despite the observed bursting/chaotic behavior of BZ, the resulting dominant morphology continues to be giant μ-sized vesicles (Fig. 6b, d stage 2). The steady-state conversion was ~40% at the two stages using residence time of 60 min, while conversion increased to ~54% in the middle stage for a residence time of 120 min.

We point out that this dynamic experiment together with some additional experiments (Supplementary Fig. 6), in which we varied the BZ recipe, constitutes, to the best of our knowledge, the first report of bursting/chaotic behavior in BZ-driven polymerization and of course in BZ–PISA.

Effect of the BZ-reactant recipe. Adjusting the concentrations of the BZ reactants provides yet another way to influence the nonlinear dynamical behaviors and the periodic radical generation that consequently affect both the polymerization and the self-assembly stages of PISA. In an effort to assess the possibility to tune the recipe of the BZ reaction in CSTR to regulate self-assembly in CSTR, we used a different BZ recipe (0.45 mM Ru-catalyst recipe, see Supplementary Table 1) that is more concentrated on several reactants than the original recipe. Supplementary Fig. 7 shows the oscillations of the redox potential of the pure BZ reaction and the BZ reaction with PEG_{45}-CDTPA and monomer for a 0.45 mM Ru-catalyst recipe. Compared with the 0.2 mM Ru-catalyst recipe, the induction period was now shortened to ~20 min, the amplitude and period were decreased to 120 mV and ~35 s. Faster oscillations, i.e., faster radical generation, generally increase polymerization rate and monomer conversion as demonstrated by Fig. 7a. When a monomer/RAFT agent ratio of 200 was used, the conversion at a residence time of 60 min with 0.45 mM Ru-catalyst recipe (43.1%) matches the conversion at the residence time of 90 min with 0.2 mM Ru-catalyst recipe (41.3%) (Fig. 7a and Table 1). A mixture of micelles and short worms (Fig. 7b) was obtained over a shorter residence time of 60 min as compared with 90 min of 0.2 mM Ru-catalyst recipe, which we attribute as due to the faster oscillations, i.e., faster radical generation, accompanied by a correspondingly larger conversion.

Discussion

By coupling BZ–RAFT–PISA with a CSTR mode of operation, we have accomplished controllable and reproducible autonomous synthesis of giant vesicles (and other intended morphologies) with known and tunable chemical properties of the encapsulated cargo that fed the polymerization in the first place.

First, we observed that as the residence time is increased (for an appropriately selected monomer/RAFT concentration ratio), the larger the steady-state conversion with the steady-state dominant morphology evolving from micelles to worms, to ~100-nm vesicles, and to giant ~1-μm vesicles. Hence, the residence time acts for CSTR as the proxy of polymerization time in batch. We also proved experimentally that if the monomer/RAFT concentration ratio is decreased while keeping the same BZ recipe, then longer residence times are required to achieve self-assembled structures, i.e., it takes longer residence times to obtain micelles, worms, and vesicles, respectively. On the other hand, if the monomer/RAFT concentration ratio is kept constant and the BZ recipe is changed to concentrations leading to faster radical production and faster observed oscillations, then shorter residence times are needed to respectively achieve micelles, worms, vesicles, and giant micro-sized vesicles. In order to prove that residence time alone is an effective and convenient variable to control the self-assembly and the chemical cargo in a reproducible way, we designed and run an experiment in which residence time was first increased and then decreased to the initial value, and we verified that the conversion, the stationary oscillation features, and the dominant self-assembly first changed and then evolved back to the original stationary

conditions. Interestingly, for the stage with residence time of 120 min, a bursting/chaotic regime of BZ was observed. Hence, running BZ-driven polymerization in CSTR allows to attain not only periodic oscillatory behaviors but also more exotic, chaotic, or aperiodic oscillatory regimes. (We did not study the effects of these exotic regimes on the morphologies.)

Compared with batch BZ–PISA, our CSTR strategy offers several advantages. (1) Stationary and well-known oscillatory conditions were achieved during polymerization, thus ensuring consistency of both the self-assembly and the chemical properties of the cargo. (2) The stationary oscillatory regime, and consequently the associated stationary conversion, self-assembly, and properties of the cargo can be modified by varying residence time, DP target, and/or BZ-recipe properties, which pave the way to optimize reactor operation for the autonomous synthesis of specific self-assembled objects with desired chemical and functional properties of the entrapped cargo. (3) The rich range of aperiodic and periodic oscillatory behaviors, including bursting and chaotic regimes, which characterize BZ in CSTR operation, can be attained when coupling BZ to polymerization and PISA.

Finally, it is relevant to point out in the context of artificial biology or in the exploration of the route from protolife to the origins of life, a CSTR mode operation that resembles more closely the out-of-equilibrium and open-system characteristics of living systems and their environments. This makes our model platform suitable for the study of protolife scenarios, including pH-oscillator-based scenarios[52]. In addition, we expect that these results will apply to PISA with oscillatory chemistries other than BZ.

Methods

Materials. Chemicals were used without further treatment if not otherwise stated. Malonic acid (MA, 99%), tris(2,2′-bipyridyl)dichlororuthenium (II) hexahydrate ($Ru(bpy)_3^{2+}$), diacetone acrylamide (DAAM, 99%), poly(ethylene glycol) methyl ether (PEG_{45}-OH, average Mn~2000 g mol^{-1}), and 4-Cyano-4-[(dodecylsulfanylthiocarbonyl)sulfanyl]pentanoic acid (CDTPA, 97%) were obtained from Sigma Aldrich. Sodium bromate ($NaBrO_3$, 99.5%) was purchased from Alfa Aesar. Sulfuric acid (H_2SO_4, 10 Normal) was purchased from Ricca Chemical Company. Deuterated methanol (CD_3OD, 99.96 atom%) was purchased from Cambridge Isotope Laboratories, Inc. PEG_{45}–CDTPA macroCTA was synthesized according to the literature[48]. The ultrapure water (molecular grade) used throughout all syntheses was purchased from Hardy Diagnostic.

Characterization. ^{1}H NMR spectra were recorded on a Varian Unity/Inova 500B spectrometer (500 MHz) at room temperature. The concentrated solution or solid polymer was dissolved in methanol-d_4 for ^{1}H NMR measurement. GPC analysis was performed using an Agilent 1260 system. The eluent was *N*,*N*-dimethylformamide (HPLC grade, containing 50 mM LiBr) at a flow rate of 1 mL min^{-1} at 50 °C. Polystyrene (PS) standard was used to calibrate GPC for molecular weight measurements. TEM images were obtained on a JEOL 2100 electron microscope and Hitachi HT7800 microscope at an acceleration voltage of 80 kV. The samples were prepared by dropping 5 µL of solution on carbon-coated copper grids (200 mesh, Ted Pella, USA) and left to stay for 1 min without adding additional stain agent since the Ru^{2+} in the solution provides enough contrast. The excess solution was blotted carefully with filter paper. DLS measurements were carried out using a Beckman–Coulter Delsa^{TM} Nano C Particle Size & Zeta Potential Analyzer and Malvern Panalytical, Zetasizer Nano ZS. CLSM images were obtained using an ELYRA super-resolution microscope. The samples were stained with 0.4 mM Rhodamine 6 G (v/v 10:1) and were excited at 561 nm. Ultraviolet–visible (UV–Vis) spectroscopy measurements were conducted on a Cole Parmer 2100UV + spectrophotometer. In total, 20-µL samples were diluted with 5 mL of methanol for UV–vis measurement.

Experimental setup. As shown in Fig. 1, the feeding system was manually programmed to automatically calculate and deliver the appropriate inflow of a macro PEG–CTA, monomer, and BZ reactants into the system and the outflow to keep the volume constant and the desired residence time. Each reactant (PEG_{45}–CDTPA, DAAM, H_2SO_4 + Malonic Acid, $Ru(bpy)_3^{2+}$, and $NaBrO_3$) was pumped to the reactor by a Longer BT-100 2J peristaltic pump. The same type of peristaltic pump was used to pump the outflow. Oscillations were continuously monitored by measuring the redox potential (Ru^{2+}/Ru^{3+}) with a Microelectrodes Inc ORP meter (with data frequency of five samples per second). A jacketed glass reactor was connected to a thermal bath to keep the reaction temperature constant at 25 °C, and a magnetic stirrer was used for stirring the solution.

B–Z-mediated RAFT aqueous dispersion PISA in CSTR. Reactant concentrations for recipe 1 are as follows: PEG_{45}–CDTPA (0.08 mM), Ru $(bpy)_3^{2+}$ (0.2 mM), DAAM (32 mM), $NaBrO_3$ (0.15 M), H_2SO_4 (0.5 M), and $CH_2(COOH)_2$ (0.06 M) for a target degree of polymerization of 400. The total volume is 50 mL. The contents were stirred at 300 rpm at 25 °C in dark conditions (note that the ruthenium catalyst is photosensitive).

Residence time distribution measurements. Residence time distribution measurements using a pulse method are nontrivial to carry out in the BZ reaction medium, due to the extreme reactivity of BZ and the lack of inert tracers. BZ is acidic and pH sensitive and contains a strong oxidant and a metallic catalyst. Since the tracer should be inert, any molecule that affects pH or redox potential or reacts with the radicals produced during reaction is not an adequate tracer. Most organic fluorescent dyes are degraded or oxidized by BZ, pH dyes would affect pH, most salts would affect the redox potential, etc. Due to the difficulty to find an appropriate tracer, we ran tracer tests in our setup running water instead of the BZ to get a baseline, before running the same tests with BZ and evaluate the degree of degradation of the tracer. Supplementary Fig. 3 shows the tracer results using a pulse, leading to a concentration of 3.4 µg ml^{-1} of Rhodamine B and measuring the absorbance at a wavelength of 543 nm, for residence times of 60 and 120 min. As shown in Supplementary Fig. 3, the actual residence time distributions are very close to their respective ideal RTDs. The experimental mean RTD and variance RTD in water are 57 and 54 for the 60-min setting and 116 and 116 min for the 120-min setting.

Unfortunately, when attempting the RTD measurement in the actual reaction medium, BZ polymerization, even if using a ten times more concentrated pulse of the same tracer, Rhodamine B, the tracer was completely degraded and reacted within 3 min, illustrating the difficulty to run RTD measurements in BZ (see Supplementary Fig. 4).

Data availability

The datasets generated and/or analyzed during this study are available from the corresponding author on reasonable request.

Received: 9 May 2019; Accepted: 13 November 2019;
Published online: 09 December 2019

References

1. Discher, D. E. & Eisenberg, A. Polymer vesicles. *Science* **297**, 967–973 (2002).
2. Discher, B. M. et al. Polymersomes: tough vesicles made from diblock copolymers. *Science* **284**, 1143–1146 (1999).
3. Mason, A. F. & Thordarson, P. Polymersomes as protocellular constructs. *J. Polym. Sci. A* **55**, 3817–3825 (2017).
4. Albertsen, A. N., Szymański, J. K. & Pérez-Mercader, J. Emergent properties of giant vesicles formed by a polymerization-induced self-assembly (PISA) reaction. *Sci. Rep.* **7**, 41534 (2017).
5. Buddingh', B. C. & van Hest, J. C. M. Artificial cells: synthetic compartments with life-like functionality and adaptivity. *Acc. Chem. Res.* **50**, 769–777 (2017).
6. Kamat, N. P., Katz, J. S. & Hammer, D. A. Engineering polymersome protocells. *J. Phys. Chem. Lett.* **2**, 1612–1623 (2011).
7. Palivan, C. G. et al. Bioinspired polymer vesicles and membranes for biological and medical applications. *Chem. Soc. Rev.* **45**, 377–411 (2016).
8. Gaitzsch, J., Huang, X. & Voit, B. Engineering functional polymer capsules toward smart nanoreactors. *Chem. Rev.* **116**, 1053–1093 (2015).
9. Antonietti, M. & Förster, S. Vesicles and liposomes: a self-assembly principle beyond lipids. *Adv. Mater.* **15**, 1323–1333 (2003).
10. Rideau, E., Dimova, R., Schwille, P., Wurm, F. R. & Landfester, K. Liposomes and polymersomes: a comparative review towards cell mimicking. *Chem. Soc. Rev.* **47**, 8572–8610 (2018).
11. Che, H. & van Hest, J. C. M. Stimuli-responsive polymersomes and nanoreactors. *J. Mater. Chem. B* **4**, 4632–4647 (2016).
12. Hu, X. et al. Stimuli-responsive polymersomes for biomedical applications. *Biomacromolecules* **18**, 649–673 (2017).
13. Zhua, Y., Yang, B., Chen, S. & Du, J. Polymer vesicles: mechanism, preparation, application, and responsive behavior. *Prog. Polym. Sci.* **64**, 1–22 (2017).
14. Charleux, B., Delaittre, G., Rieger, J. & D'Agosto, F. Polymerization-induced self-assembly: from soluble macromolecules to block copolymer nano-objects in one step. *Macromolecules* **45**, 6753–6765 (2012).
15. Warren, N. J. & Armes, S. P. Polymerization-induced self-assembly of block copolymer nanoobjects via RAFT aqueous dispersion polymerization. *J. Am. Chem. Soc.* **136**, 10174–10185 (2014).
16. Varlas, S. et al. Photoinitiated polymerization-induced self-assembly in the presence of surfactants enables membrane protein incorporation into vesicles. *Macromolecules* **51**, 6190–6201 (2018).

17. LoPresti, C., Lomas, H., Massignani, M., Smart, T. & Battaglia, G. Polymersomes: nature inspired nanometer sized compartments. *J. Mater. Chem.* **19**, 3576–3590 (2009).
18. Canning, S. L., Smith, G. N. & Armes, S. P. A critical appraisal of RAFT-mediated polymerization-induced self-assembly. *Macromolecules* **49**, 1985–2001 (2016).
19. Cheng, G. & Pérez-Mercader, J. Polymerization-induced self-assembly for artificial biology: opportunities and challenges. *Macromol. Rapid Commun.* **409**, 1800513 (2018).
20. Yeow, J. & Boyer, C. Photoinitiated polymerization-induced self-assembly (photo-PISA): new insights and opportunities. *Adv. Sci.* **4**, 1700137–1700152 (2017).
21. Bastakoti, B. & Pérez-Mercader, J. Facile one-pot synthesis of functional giant polymeric vesicles controlled by oscillatory chemistry. *Angew. Chem. Int. Ed.* **56**, 12086–12091 (2017).
22. Bastakoti, B. & Pérez-Mercader, J. Autonomous ex novo chemical assembly with blebbing and division of functional polymer vesicles from a "homogeneous mixture". *Adv. Mater.* **29**, 1704368–1704373 (2017).
23. Belousov, B. P. A periodic reaction and its mechanism. *Compilation of Abstracts on Radiation Medicine*. 145–147 (1958).
24. Ball, P. *The Self-Made Tapestry: Pattern Formation in Nature*. (Oxford University Press, Oxford, 1999).
25. Field, R. J., Körös, E. & Noyes, R. M. Oscillations in chemical systems: thorough analysis of temporal oscillation in the bromate-cerium-malonic acid system. *J. Am. Chem. Soc.* **94**, 8649–8664 (1972).
26. Váradi, Z. & Beck, M. T. Inhibition of a homogeneous periodic reaction by radical scavengers. *J. Chem. Soc. Chem. Commun.* **2**, 30–31 (1973).
27. Försterling, H. D., Muranyi, S. & Noszticzius, Z. Evidence of malonyl radical controlled oscillations in the Belousov-Zhabotinskii reaction (malonic acid-bromate-cerium system). *J. Phys. Chem.* **94**, 2915–2921 (1990).
28. Washington, R. P., West, W. W., Misra, G. P. & Pojman, J. A. Polymerization coupled to oscillating reactions: (1) a mechanistic investigation of acrylonitrile polymerization in the Belousov-Zhabotinsky reaction in a batch reactor. *J. Am. Chem. Soc.* **121**, 7373–7380 (1999).
29. Pérez-Mercader, J. & Dueñas-Díez, M., Case D. US Patent US9582771B2 Issued 2017.
30. Dueñas-Díez, M. & Pérez-Mercader, J. How chemistry computes: language recognition by non-biochemical chemical automata. From finite automata to turing machines. *iScience* **19**, 514–526 (2019).
31. Graziani, K. R., Hudson, J. L. & Schmitz, R. A. The Belousov-Zhabotinskii reaction in a continuous flow reactor. *Chem. Eng. J.* **12**, 9–21 (1976).
32. Schmitz, R. A., Graziani, K. R. & Hudson, J. L. Experimental evidence of chaotic states in the Belousov-Zhabotinskii reaction. *J. Chem. Phys.* **67**, 3040–3044 (1977).
33. Rossler, O. E. & Wegmann, K. Chaos in the Zhabotinskii reaction. *Nature* **271**, 89 (1978).
34. Scott, S. K. *Chemical Chaos*. (Oxford University Press, 1993).
35. Field, R. J. Chaos in the Belousov-Zhabotinsky reaction. *Mod. Phys. Lett. B* **29**, 1530015 (2015).
36. Rachwalska, M. & Kawczyński, A. L. Regularities in complex transient oscillations in the Belousov-Zhabotinsky reaction in a CSTR. *J. Phys. Chem. A* **101**, 1518–1522 (1997).
37. Srivastava, R., Dueñas-Díez, M. & Pérez-Mercader, J. Feed rate noise modulates autocatalysis and shapes the oscillations of the Belousov-Zhabotinsky reaction in a continuous stirred tank reactor. *Reaction Chem. Eng.* **3**, 216–226 (2018).
38. Eckardt, O., Wenn, B., Biehl, P., Junkers, T. & Schacher, F. H. Facile photo-flow synthesis of branched poly(butyl acrylate)s. *Reaction Chem. Eng.* **2**, 479–486 (2017).
39. Junkers, T. Precision polymer design in microstructured flow reactors: improved control and first upscale at once. *Macromol. Chem. Phys.* **218**, 1600421 (2017).
40. Zaquen, N., Yeow, J., Junkers, T., Boyer, C. & Zetterlund, P. B. Visible light-mediated polymerization-induced self-assembly using continuous flow reactors. *Macromolecules* **51**, 5165–5172 (2018).
41. Zaquen, N. et al. Scalable aqueous RAFT Photo polymerization-induced self-assembly of acrylamides for direct synthesis of polymer nanoparticles for potential drug delivery applications. *ACS Appl. Polym. Mater.* **1**, 1251–1256 (2019).
42. Zaquen, N. et al. Rapid oxygen tolerant aqueous RAFT photopolymerization in continuous flow reactors. *Macromolecules* **52**, 1609–1619 (2019).
43. Zaquen, N. et al. Alcohol-based PISA in batch and flow: exploring the role of photoinitiators. *Polym. Chem.* **10**, 2406–2414 (2019).
44. Parkinson, S., Hondow, N. S., Conteh, J. S., Bourne, R. A. & Warren, N. J. All-aqueous continuous-flow RAFT dispersion polymerisation for efficient preparation of diblock copolymer spheres, worms and vesicles. *Reaction Chem. Eng.* **4**, 852–861 (2019).
45. Corrigan, N., Zhernakov, L., Hashim, M. H., Xu, J. & Boyer, C. Flow mediated metal-free PET-RAFT polymerisation for upscaled and consistent polymer production. *Reaction Chem. Eng.* **4**, 1216–1228 (2019).
46. Bamforth, J. R., Merkin, J. H., Scott, S. K., Toth, R. & Gaspar, V. Flow-distributed oscillation patterns in the Oregonator model. *Phys. Chem. Chem. Phys.* **3**, 1435–1438 (2001).
47. Kærn, M. & Menzinger, M. Experiments on flow-distributed oscillations in the Belousov-Zhabotinsky reaction. *J. Phys. Chem. A* **106**, 4897–4903 (2002).
48. Xu, X., Smith, A. E., Kirkland, S. E. & McCormick, C. L. Aqueous RAFT synthesis of pH-responsive triblock copolymer mPEO-PAPMA-PDPAEMA and formation of shell cross-linked micelles. *Macromolecules* **41**, 8429–8435 (2008).
49. Byard, S. J., Williams, M., McKenzie, B. E., Blanazs, A. & Armes, S. P. Preparation and cross-linking of all-acrylamide diblock copolymer nano-objects via polymerization-induced self-assembly in aqueous solution. *Macromolecules* **50**, 1482–1493 (2017).
50. Zhou, W., Qu, Q., Xu, Y. & An, Z. Aqueous polymerization-induced self-assembly for the synthesis of ketone-functionalized nano-objects with low polydispersity. *ACS Macro Lett.* **4**, 495–499 (2015).
51. Chan, N., Cunningham, M. F. & Hutchinson, R. A. Continuous controlled radical polymerization of methyl acrylate with copper wire in a CSTR. *Polym. Chem.* **3**, 486–497 (2012).
52. Guo, J., Poros-Tarcali, E. & Pérez-Mercader, J. Evolving polymersomes autonomously generated in and regulated by a semibatch pH oscillator. *Chem. Commun.* **55**, 9383–9386 (2019).

Acknowledgements

We thank Repsol S.A. for supporting this research. The funders had no role in study design, data collection and analysis, decision to publish, or preparation of the paper. The authors thank Drs. Bishnu Bastakoti, Jinshan Guo, Eszter Poros-Tacali, Gong Cheng, Shaji Varghese, and Chenyu Lin for discussions and useful suggestions.

Author contributions

L.H. and M.D.D. performed the experiments; L.H., M.D.D., and J.P.M. analyzed the results; L.H., M.D.D., and J.P.M. designed the experiments and methods; L.H., M.D.D., and J.P.M. wrote the paper and Supplementary Information; R.S., M.D.D., and J.P.M. conceived the initial idea; J.P.M. directed the project.

Competing interests

The authors declare no competing interests.

Additional information

Supplementary information is available for this paper at https://doi.org/10.1038/s42004-019-0241-1.

Correspondence and requests for materials should be addressed to M.D.-D. or J.P.-M.

Reprints and permission information is available at http://www.nature.com/reprints

Publisher's note Springer Nature remains neutral with regard to jurisdictional claims in published maps and institutional affiliations.